

## Article

# Dynamical Sensitivity of Three-Layer Micro Electromechanical Systems to the Optical Properties of the Intervening Liquid Layer

Fatemeh Tajik <sup>1,\*</sup> and George Palasantzas <sup>2</sup> <sup>1</sup> Department of Condensed Matter Physics, Faculty of Physics, Alzahra University, Tehran 1993891167, Iran<sup>2</sup> Zernike Institute for Advanced Materials, University of Groningen, Nijenborgh 4, 9747 AG Groningen, The Netherlands; g.palasantzas@rug.nl

\* Correspondence: f.tajik@alzahra.ac.ir

**Abstract:** Here, we investigate the actuation dynamics of a micro device with different intervening liquids between the actuating components under the influence of Casimir and dissipative hydrodynamic forces. This is enabled via phase space portraits, which demonstrate that by increasing the dielectric response of the intervening layer the autonomous device may not come into stiction due to the decreasing in magnitude Casimir force. Unlike the micro devices that are placed in vacuum with an intervening liquid, the phase portraits show only a spiral trajectory which eventually stops at a rest position due to the strong energy dissipation by the position dependent hydrodynamic drag forces, even when considering sufficiently strong restoring forces. Moreover, it is feasible to expand the area of motion using intervening liquids with lower dynamic viscosity or increasing the slip length of the intervening fluid. Finally, under the influence of an external driven force, which is the realistic case for possible applications, the system can reach stable oscillation at larger separations with an amplitude higher for the liquid that led to lower Casimir and hydrodynamic forces. Hence, the results presented in this study are essential for studying the dynamical behavior of MEMS and their design in liquid environments.

**Keywords:** Casimir effect; hydrodynamic force; MEMS; NEMS; actuation dynamics; stiction



**Citation:** Tajik, F.; Palasantzas, G. Dynamical Sensitivity of Three-Layer Micro Electromechanical Systems to the Optical Properties of the Intervening Liquid Layer. *Physics* **2023**, *5*, 1081–1093. <https://doi.org/10.3390/physics5040070>

Received: 27 September 2023

Revised: 19 October 2023

Accepted: 27 October 2023

Published: 21 November 2023



**Copyright:** © 2023 by the authors. Licensee MDPI, Basel, Switzerland. This article is an open access article distributed under the terms and conditions of the Creative Commons Attribution (CC BY) license (<https://creativecommons.org/licenses/by/4.0/>).

## 1. Introduction

During the past decades the emergence of rapid development in micro/nano fabrication has led to scaling down of electromechanical systems into submicron-length scales. This opens new areas for the application of the Casimir forces, since they could inevitably play role in the operation of micro/nano systems [1–8]. These devices have sufficiently large surface areas and gaps small enough for the Casimir force to pull components together leading to permanent adhesion, a phenomenon known as stiction [9–12]. This malfunction in many cases is unavoidable for the dynamical stability of micro/nano electromechanical systems (MEMS/NEMS) such as sensors, micro switches, actuators. Hence, a comprehensive knowledge about the magnitude and direction of the Casimir force can provide strong insight into the design and architecture of MEMS/NEMS.

The Casimir force, which originates from perturbations of fluctuating electromagnetic (EM) fields [13,14], was discovered in 1948 by the Dutch physicist Hendrick Casimir [15]. This is a quantum mechanical attractive force between two parallel, neutral, and perfectly conducting flat plates, and without considering thermal fluctuations (at temperature  $T = 0$  K) [15]. In the 1950s, Evgeny Lifshitz and collaborators proposed the general theory for the Casimir force between parallel flat plates made of real dielectric materials [16]. For this purpose, the fluctuation–dissipation theorem was utilized to relate the dissipative properties of the plates (optical absorption by many microscopic dipoles) and EM fluctuations. The Lifshitz theory predicts the attractive force between the two parallel plates of arbitrary

materials and covers both at short ranges (non-retarded regime) the van der Waals forces, and at longer ranges (retarded regime) the Casimir forces. [16,17].

Furthermore, the Lifshitz theory enables the prediction of the actuation dynamics of micro/nano devices actuation since the omnipresent Casimir force could play a significant role. This is because the Lifshitz theory allows to compute the tuning of the Casimir force, actually, for both the magnitude and direction, by a suitable choice of the interacting materials with the necessary optical properties [18–21]. As a result, several studies have been performed on the effect of optical properties on the actuation dynamic of devices in order to widen the range of their applications [22–25]. For example, in Ref. [23], it was illustrated how the use of phase change materials can delay chaotic motion in MEMS without changing the materials. Also, in Ref. [24], it was investigated how one can decrease the influence of the temperature on the magnitude of the Casimir force with the use of suitable materials in order to survive operation at low or high temperatures. Finally, in Ref. [25], it was demonstrated how the magnetoelectric effect in micro devices consisting of topological insulators can become dominant on the operation of MEMS and taking into account its sensitive dependence on thermal fluctuations.

Actually, a three-layer system consisting of two actuating components immersed inside a liquid has attracted extensive attention because it provides unique advantages. In this system, under certain conditions, it is possible to generate repulsive Casimir forces leading to stable operation without employing a restoring mechanical spring [26–36]. Moreover, with a ferrofluid between the actuating components one can open new opportunities in nanotechnology [29], for instance, in micromechanical sensors [30], microfluidics [31,36], and micro robotics [37]. Therefore, we consider here a MEMS operating inside a fluid, and the main aim is to investigate how stable operation is sensitive to optical properties of the intervening layer by taking also into account the dynamic viscosity of the intervening fluids as well as the fluid slip length on the walls of the actuating plate. Hence, the results presented in this study are essential for studying the dynamical behavior of MEMS and their design in liquid environments.

## 2. Methods and Materials

Here, we assume that the actuating components of the MEMS device are coated with Au, which is a good conductor. The latter has static conductivity  $\omega_p^2/\omega_\tau|_{Au} \approx 1600$  eV [38] ( $\omega_p$  and  $\omega_\tau$  define the plasma and relaxation frequencies, respectively), and it is also extensively used for Casimir force measurements. Moreover, ethanol and kerosene are used as the intervening layer between the Au plates. Previous studies have shown that ethanol could produce repulsive Casimir forces in a system consisting of different interacting bodies (with dielectric functions  $\epsilon_{Liquid}$ ,  $\epsilon_1$ ,  $\epsilon_2$ , respectively) if the condition  $\epsilon_1 < \epsilon_{Liquid} < \epsilon_2$  is satisfied [26–28], and kerosene is also used in ferrofluid-based microdevices. In any case, both materials, as an intervening medium, have attracted attention in investigations related to Casimir forces [29–32]. The dielectric response of ethanol at imaginary frequencies can be described by a three-oscillator Ninham–Parsegian model [29]:

$$\epsilon_E(i\zeta) = 1 + \frac{\epsilon_0 - \epsilon_{IR}}{1 + (\zeta/\omega_{MW})} + \frac{\epsilon_{IR} - (n_0)^2}{1 + (\zeta/\omega_{IR})^2} + \frac{(n_0)^2 - 1}{1 + (\zeta/\omega_{UV})^2}, \tag{1}$$

where  $\zeta$  is the Matsubara frequency,  $n_0 = 1.35$  is the refractive index in the visible range,  $\epsilon_0 = 25.07$  is the static dielectric constant, and  $\epsilon_{IR} = 4.2$  is the dielectric constant where the microwave (MW) relaxation ends and the infrared (IR) begins.  $\omega_{MW} = 6.97 \times 10^9$  rad/s,  $\omega_{IR} = 2.588 \times 10^{14}$  rad/s, and  $\omega_{UV} = 1.924 \times 10^{16}$  rad/s are the characteristic MW, IR, and ultraviolet (UV) absorption frequencies, respectively. Similarly, one has for the dielectric function of kerosene at imaginary frequencies [29]:

$$\epsilon_K(i\zeta) = 1 + \frac{B}{1 + (\zeta\tau)} + \frac{C_{IR}}{1 + (\zeta/\omega_{IR})^2} + \frac{C_{UV}}{1 + (\zeta/\omega_{UV})^2}, \tag{2}$$

where the second term on the right-hand side describes the contribution to the dielectric permittivity from the orientation of permanent dipoles. The values of  $B = 0.020$  and  $1/\tau = 8.0 \times 10^8$  rad/s were determined from the measured data of Ref. [38] in the MW region. The third term shows the effect of ionic polarization with  $C_{IR} = 0.007$  and  $\omega_{IR} = 2.14 \times 10^{14}$  rad/s as obtained using the infrared optical data of Ref. [39]. The fourth term describes the optical data in the UV region with the values  $C_{UV} = 0.773$  (obtained from the static dielectric permittivity at zero frequency  $\epsilon_K = 1.8$  [38] since  $\epsilon_K = 1 + B + C_{IR} + C_{UV}$ ) and  $\omega_{UV} = 1.0 \times 10^{16}$  rad/s. Finally, the dielectric functions,  $\epsilon(i\zeta)$ , of all media at imaginary frequencies, which are vital as input for the calculations of the Casimir force via the Lifshitz theory, are shown in Figure 1a.

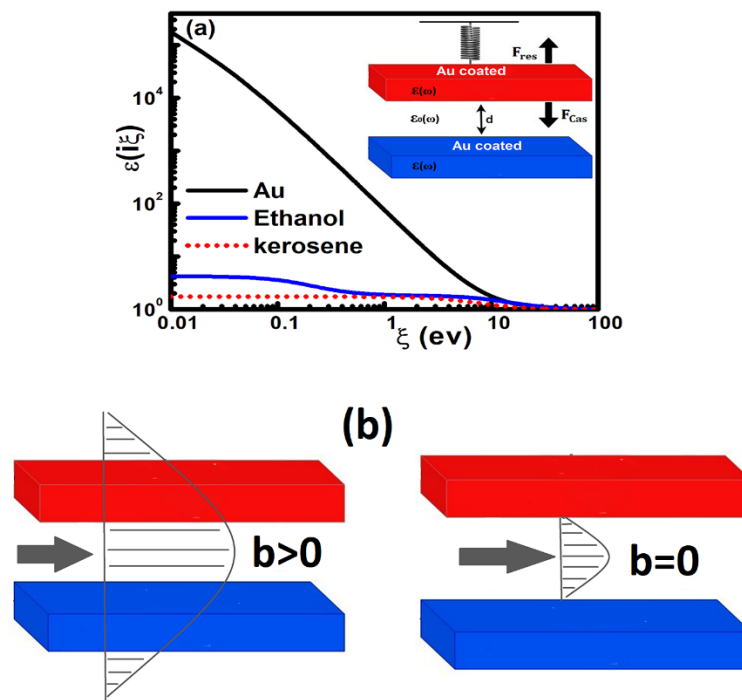


**Figure 1.** (a) Dielectric functions  $\epsilon(i\zeta)$  of imaginary Matsubara frequencies for the materials considered in this study. The inset shows the MEMS design for this study. (b) Schematic of three-layer Au micro system with no-slip/slip (having slip length,  $b$ ) boundary conditions. See text for details.

The dielectric function  $\epsilon(i\zeta)$  is a vital input function to compute the Casimir force using the Lifshitz theory [16]. The Casimir force between two parallel plates at  $T = 300$  K is given in terms of the Lifshitz theory (at the imaginary frequency representation) by the equation

$$F(T, z) = \frac{kT}{\pi} \sum'_{n=0} \int_0^\infty dq q |k_0| g(q, i\zeta_n), \tag{3}$$

where  $z$  denotes the separation,  $q$  denotes the in-plane vector, the imaginary frequencies ( $\zeta$ ) describe the discrete Matsubara frequencies ( $\zeta = 2\pi kTn/\hbar$ ). Here,  $\hbar$  is the reduced Planck's constant,  $k$  denotes the Boltzmann constant, and the prime in the sum of Equation (3) means that the  $n = 0$  term must be taken with half weight. The term  $g(q, i\zeta_n)$  describes the multiple reflections from the inner surfaces of the interacting bodies, which is represented by the equation

$$g(q, i\zeta_n) = \sum_{\nu=s,p} r_1^\nu r_2^\nu e^{-2k_0 z} / (1 - r_1^\nu r_2^\nu e^{-2k_0 z}), \tag{4}$$

where the Fresnel reflection coefficients are given by

$$r_i^s = (k_0 - k_i) / (k_0 + k_i) \tag{5}$$

and

$$r_i^p = (\epsilon_i k_0 - \epsilon_0 k_i) / (\epsilon_i k_0 + \epsilon_0 k_i) \tag{6}$$

where the superscript “s” indicates the transverse electric polarization (TE), and the subscript “p” indicates the transverse magnetic polarization (TM) of the electromagnetic field, respectively.  $\epsilon_0(i\zeta)$  and  $\epsilon_i(i\zeta)$  are the dielectric functions of the intervening layer and the interacting components, respectively.  $k_i = \sqrt{\epsilon_i(i\zeta) \zeta^2 / c^2 + q^2}$  ( $i = 0,1,2$ ) describes the out-of-plane wave vector in the intervening layer between the interacting components ( $k_0$ ), and in each of the interacting components ( $k_{i=1,2}$ ),  $c$  is the speed of light, and  $q$  is the in-plane wave vector.

Moreover, we consider a typical MEMS, which is shown in the inset of Figure 1a, consisting of two plates with the upper one being able to move. Both components are assumed to be coated with Au, (with a coating thickness of more than 100 nm in order to be considered optically bulk material) [40]. Moreover, we assume flat plates because, at short separations ( $\ll 100$  nm), nanoscale roughness can significantly affect the Casimir force. The initial distance of the parallel plates is assumed to be  $d = 300$  nm, and the system temperature being  $T = 300$  K. The intervening medium between these components is assumed to be ethanol or kerosene. The equation of motion for the MEM system without any external driven force is given by

$$M \frac{d^2z}{dt^2} + \left( \frac{M\omega_0}{Q} \right) \frac{dz}{dt} = F_{res} + F_{Cas} + F_h, \tag{7}$$

where  $M$  is the mass of the moving plate. The term  $(M\omega_0/Q)(dz/dt)$  describes the Stokes term for the energy losses of the moving plate, whereas  $Q$  defines the quality factor of the MEMS (in this study,  $Q = 400$  is considered, while the calculations performed with low values of  $Q = 10$  do not have significant effect). We also assume  $\omega = 300$  kHz, which is a typical frequency for Atomic Force Microscopy cantilevers and MEMS [41].  $F_{res}(z) = -k(d - z)$  is the restoring force, where  $k$  is the elastic spring stiffness, and  $F_{Cas}(z)$  is the Casimir force, which is computed via the Lifshitz theory. Finally,  $F_h$  defines the separation-dependent hydrodynamic force, which is the dominant dissipation term due to its  $1/z$  dependence at short separations, and it is given by [42–51]

$$F_h(z) = -\frac{A\mu}{z} \frac{dz}{dt} f^*, \tag{8}$$

where  $A$  is the area of the plates, and we consider for both the length ( $L_x$ ) and width ( $L_y$ ) of the plates the value of  $10\mu\text{m}$ .  $\mu$  is the dynamic viscosity of the intervening liquid. The latter at 300 K has the value  $\mu = 0.001$  kg/ms and  $\mu = 0.0016$  kg/ms for ethanol and kerosene, respectively.  $f^*$  is the correction due to deviations from the Reynolds flow because of fluid slip on solid surfaces (see Figure 1b). In this study we consider the same slip length  $b$  on the surface of both plates. If  $b = 0$  then  $f^* = 1$ , otherwise it is given by [42–51]

$$f^* = \frac{1}{4} \left\{ 1 + \frac{3z}{2b} \left[ \left( 1 + \frac{z}{4b} \right) \left( 1 + \frac{4b}{z} \right) - 1 \right] \right\}. \tag{9}$$

Equation (8) is valid for fluid flow with low Reynolds numbers and short separations between the interacting components.

### 3. Results and Discussion

Before analyzing the actuation dynamics, we illustrate the influence of the optical properties of the intervening layer on the Casimir force via Lifshitz theory calculations. In order to achieve the aim, we introduce the reduction factor  $\eta_p(z)$  ( $< 1$ ) to normalize the Casimir force, with respect to the maximum Casimir force ( $F_C = \pi^2 \hbar c / 240z^4$ ) [15] between ideal metals at  $T = 0$  K. The Casimir force calculations are shown in Figure 2 and confirm that, by increasing the magnitude of the dielectric function  $\epsilon(i\zeta)$  of the intervening layer (since  $\epsilon_{Au}(i\zeta) > \epsilon_{ethanol}(i\zeta) > \epsilon_{kerosene}(i\zeta)$ ), the strength of the Casimir force is reduced.

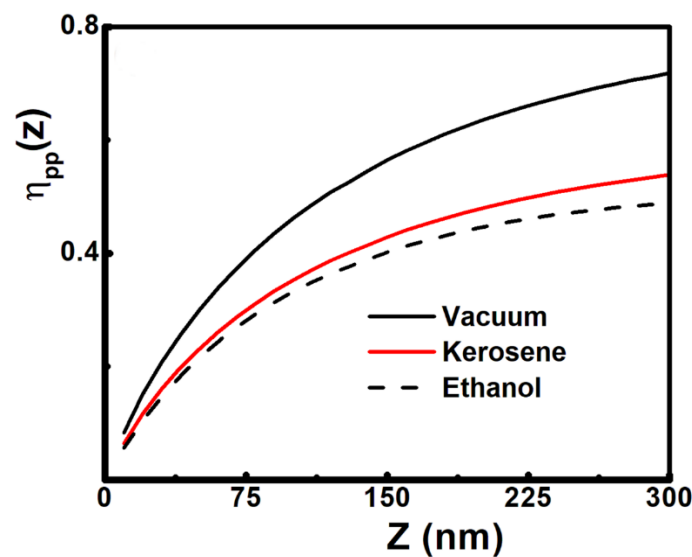


**Figure 2.** Casimir reduction factor for different three-layer micro systems versus separation between the plates. The fixed and moving components are assumed to be decorated Au with 100 nm thickness in order to be considered optically bulk. The intervening liquid layer is indicated.

Furthermore, for the discussion of the actuation dynamics for the three-layer micro device, it is helpful to consider the separation of  $z^*$ , where there is equilibrium between the Casimir and the restoring forces or  $F_c(z^*) + F_{res}(z^*) = 0$ . The latter yields the characteristic spring stiffness,  $K^* = (z^*)/(d - z^*)$ .  $d$  defines the initial separation between plates where the spring is supposed to be unstretched ( $d = 300$  nm). Indeed,  $K^*$  determines the minimum spring stiffness for the system to be able to sustain some form of motion against the stiction of the moving component on the fixed plate.

In the beginning, in order to show how the presence of the hydrodynamic drag force can change the motion and consequently the phase portrait, we have considered a micro device which is placed in vacuum or air. Under these conditions, the energy dissipation is described only by the Stokes dissipation term  $(M\omega_0/Q)(dz/dt)$ , where the values of the  $Q$  factor considered here are typical for a multitude of MEMS/NEMS operating in vacuum [4,41]. Figure 3 shows the corresponding phase portraits for a microsystem consisting of Au coated components that are placed in vacuum. As it can be seen in Figure 3a, when the stiffness of the restoring force is sufficiently strong the phase portrait reveals closed orbits, which correspond to periodic motion around a stable center equilibrium point. Also, by decreasing the magnitude of the restoring force for lower stiffness, the size of orbits enlarges, allowing the moving plate to come rather close to the fixed plate and preserve its stable operation. Notably, the stable operation can be preserved until the restoring force is stronger than the force corresponding to  $K^*$  for a considered initial condition. Hence, if the restoring force becomes smaller than the force corresponding to  $K^*$ , there is no more closed orbit. Indeed, according to Figure 3b, by considering a weak value of the restoring force ( $K < K^*$ ), it can be seen that the close orbit changes into an open orbit, which is the evidence of motion of the moving plate towards the fixed one, leading to irreversible adhesion between the components. This phenomenon is called stiction. If, however, the restoring force is increased, the dissipation energy, or equivalently the quality factor  $Q$  is decreased, then it is still possible to decrease the possibility to drive the system into stiction. The effect of the finite value of  $Q$ , due to intrinsic and extrinsic dissipation mechanisms of the oscillating plate, is shown in Figure 3b. Indeed, calculations illustrate that the transition from unstable motion towards stiction to stable oscillation is possible if dissipative motion takes place. Therefore, proper tuning of the system  $Q$  factor can also aid to prevent the permanent adhesion of an otherwise unstable micro system.

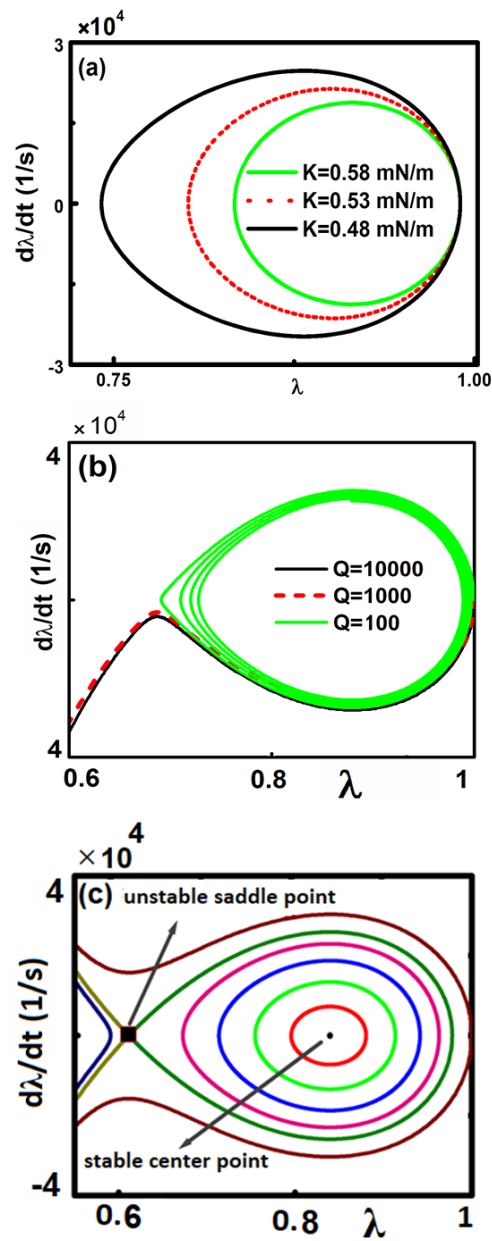


**Figure 3.** Phase portraits for micro system coated with Au.  $Q = 10,000$ ,  $\lambda = 0.95$  ( $\lambda = z^*/d$ ),  $d = 300$  nm, and  $K^* = 0.000465$  are used. (a)  $K \gg K^*$ , where the value of  $K$  is indicated. (b) Influence of the damping term on the actuation dynamics of the Au–Au micro device with  $K = 0.000464$  ( $K < K^*$ ), and different values of the quality factor  $Q$  as indicated. The closed orbits indicate stable motion, while an open orbit is the sign of unstable motion leading to stiction. (c) Phase portraits for  $K = 0.000465$  ( $K = K^*$ ), and initial conditions inside and outside the homoclinic orbit. The stable center point and unstable saddle point are indicated. See text for details.

Figure 3a,b is considered with an initial condition ( $z = 0.95d$ ) and for different values of the stiffness for the restoring force ( $K < K^*$  and  $K > K^*$ ). In Figure 3c, a fixed stiffness  $K$  (which corresponds to  $z = 0.95d$ ) is assumed, and different initial conditions are considered. According to Figure 3c, there is a homoclinic orbit, including one unstable equilibrium point on the sharp side of the orbit and one stable equilibrium inside it. This homoclinic curve can sharply separate unstable motion (leading to stiction within one period) from the periodic closed orbits around the stable center point. Any solution of the equation of motion with initial conditions within the homoclinic orbit that goes until the unstable saddle point (square in shape in Figure 3c) will lead to stable periodic motion around the

stable center. However, for any other initial conditions outside of the homoclinic orbit, the upper plate will perform unstable motion, leading to collapse on the fixed plate. In the latter case, the micro system is unstable during oscillation around these points due to the stronger Casimir force which leads to the collapse of the moving plate on the fixed one. The periodic solutions indicate that the restoring force is strong enough to keep system in operation and avoid any stiction instabilities.

Further, we consider the three-layer microsystem consisting of Au-coated components within a liquid (ethanol or kerosene) playing the role of an intervening layer. In this system, besides the Stokes dissipation term  $(M\omega_0/Q) (dz/dt)$ , the additional hydrodynamic force also describes dissipation for the micro system, and consequently can play an inevitable role for the motion and phase portrait of these devices. In this case, the phase portraits related to the autonomous micro device containing liquid do not reveal closed orbits or equivalently continuous oscillation. Unlike the micro device, which is placed in vacuum, even by considering a sufficiently strong restoring force, the phase portraits show a spiral trajectory which eventually stops at the resting position  $z = d$ . This is shown in the calculations in Figure 4, where  $\lambda^* (=z^*/d) = 0.5$  is considered as an initial position to activate the actuation. If the spring stiffness is  $K > K^*$ , then for both micro systems the moving component approaches slowly the resting position toward  $z = d$  and eventually stops. By considering  $K \gg K^*$ , the corresponding curve in phase space shows that the moving component exhibits stronger velocity due to the enhancement of the restoring force. For the value of  $K < K^*$ , the moving component eventually collapses on fixed plate leading to permanent adhesion or stiction.

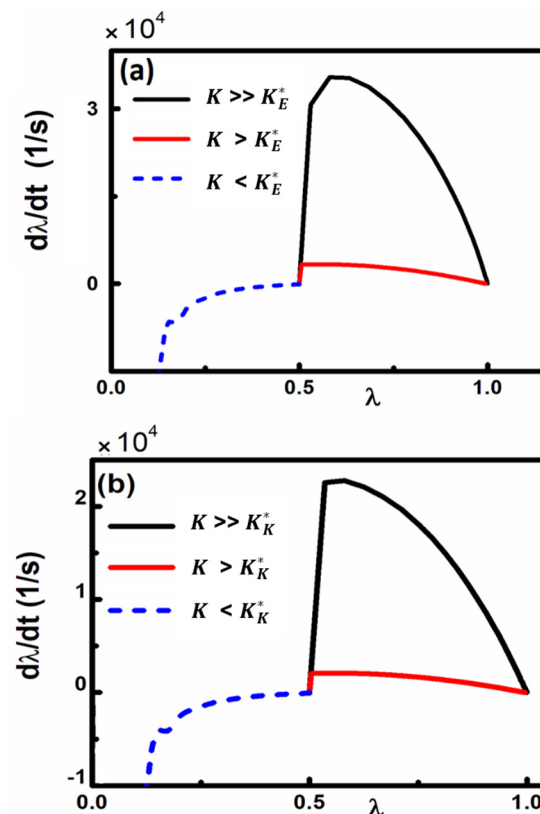


**Figure 4.** Phase portraits for the three-layer Au microsystem with (a) ethanol (b) kerosene.  $z^* = 0.5d$ ,  $d = 300$  nm, and  $b = 0$  are used. Phase space dissipative motion for various values of  $K$  (0.0005, 0.005, 0.05 N/m).  $K_E^* = 0.000635$  N/m and  $K_K^* = 0.000675$  N/m are considered for the micro systems containing ethanol and kerosene, respectively.

Further, Figure 5 shows phase space portraits using as initial condition  $\lambda^* = 0.5$  and significant spring stiffness  $K \gg K^*$ , leading to spiral trajectory towards immobility.

By increasing the restoring force, the spiral curve and consequently the velocity of the moving component becomes wider. Also, by increasing the slip length  $b$ , the hydrodynamic dissipation, which acts against the motion, reduces and, as a consequence, the spiral trajectory is more extended for both liquids. However, the effect of the slip length ( $b$ ), as the spring stiffness increases, becomes more pronounced for the micro system containing kerosene, for which the Casimir force is stronger than that of micro system containing ethanol as shown also in Figure 2. However, both micro systems preserve the ability to move if the spring stiffness  $K$  is stronger than the value that corresponds to  $\lambda^*$  ( $K_E^*$  and  $K_K^*$  for micro system containing ethanol and kerosene, respectively), while for both micro systems stiction occurs if  $K < K^*$ . Although the hydrodynamic force cannot influence the magnitude of  $K^*$  (which depends on the magnitude of the Casimir force), this term is significantly important in phase space. Indeed, as Figure 6 shows, for  $K < K^*$  the reduction of the hydrodynamic force causes the approach to stiction to take place significantly faster. Therefore, increasing the slip length ( $b$ ), or equivalently decreasing the hydrodynamic dissipation in the system containing kerosene, it is possible to make the trajectory of both micro systems similar to each other (Figure 6b).

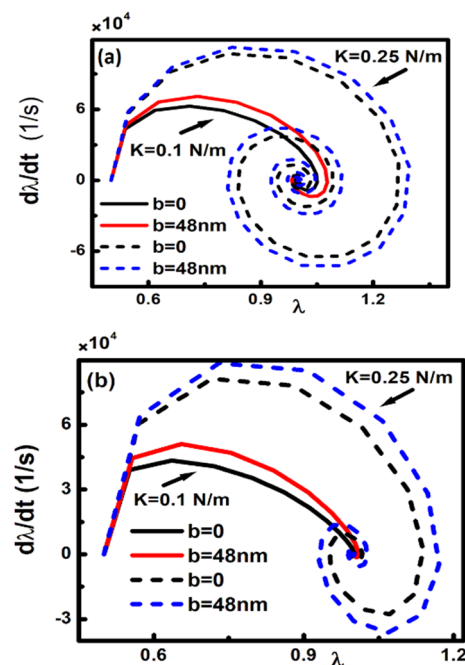


**Figure 5.** Phase portraits for the three-layer Au–Au microsystem with (a) ethanol and (b) kerosene.  $z^* = 0.5d$ ,  $d = 300$  nm, and  $K \gg K^*$  are used. The value of the slip length,  $b$ , is indicated.  $K_E^* = 0.000635$  N/m and  $K_K^* = 0.000675$  N/m are considered for the micro systems containing ethanol and kerosene, respectively.

Figure 7 compares the magnitudes of Casimir and hydrodynamic forces for a three-layer system including ethanol for the spring stiffness  $K = 0.008$  N/m. As can be seen for small and large separations, the magnitudes of both forces become comparable and consequently both forces play role in the dynamical behavior of the microsystem.

Finally, in Figure 8, we investigate the response of the three-layer micro device with a liquid as an intervening medium under the presence of an external driven periodic force ( $F(t) = F_0 \cos(\omega_d t)$ ), which is a realistic case for possible applications. In this case, the equation of motion has the more general form:

$$M \frac{d^2z}{dt^2} + \left( \frac{M\omega_0}{Q} \right) \frac{dz}{dt} = F_{res} + F_{Cas} + F_h + F_0 \cos(\omega_d t) \tag{10}$$

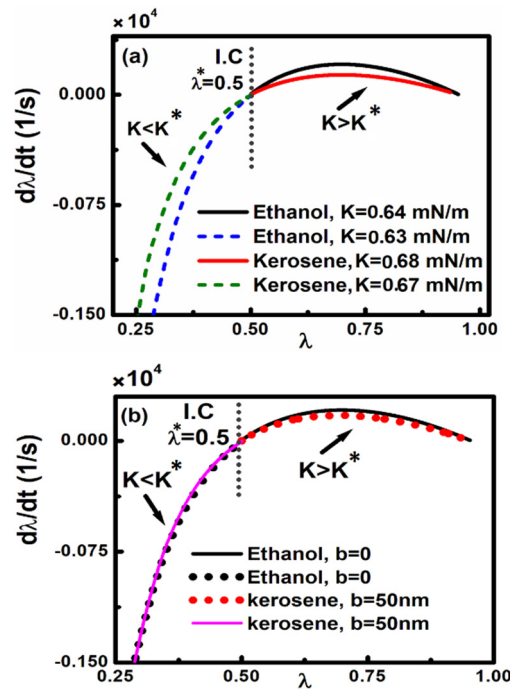


**Figure 6.** Phase portraits for the both three-layer Au microsystem with ethanol and kerosene.  $z^* = 0.5d$  and  $d = 300$  nm are used. (a)  $b = 0$  and the value of  $K$  as indicated; (b) the previous values of  $K$  are applied, and the value of slip length,  $b$ , as indicated.  $K_E^* = 0.000635$  N/m and  $K_K^* = 0.000675$  N/m are considered for the micro systems containing ethanol and kerosene, respectively.  $\lambda = 0.5$  is considered as initial condition (I.C).

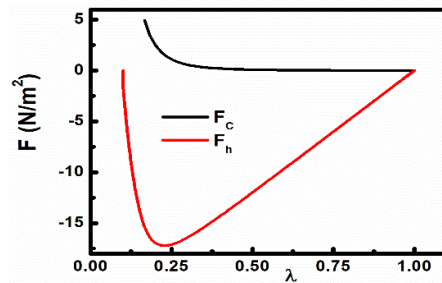


**Figure 7.** Casimir and hydrodynamic forces for the three-layer Au microsystem with ethanol.  $\lambda = z/d$  and  $d = 300$  nm are used. For computing hydrodynamic force  $z^*/d$  is considered of 0.1 and  $K = 0.008$  N/m.

By decreasing the magnitude of the Casimir force (for large value of  $\lambda$  or, equivalently, larger separations) and the hydrodynamic force, the influence of the periodic driven force becomes dominant, and the micro system can achieve continuous stable oscillation around the resting position ( $z = d$ ). Indeed, according to Figure 8a, the amplitude of the stable oscillation is higher for micro system containing ethanol due to the lower magnitude of Casimir and hydrodynamic forces. This is also depicted in Figure 8b,c, where the amplitude of the continuous oscillation is smaller in the micro system containing kerosene due to the stronger magnitude of the Casimir force and hydrodynamic force. Moreover, as Figure 8b,c indicate, an increasing amplitude of the external driven periodic force ( $F_0$ ) leads to significant influence on the continuous oscillation, while decreasing the hydrodynamic force (by increasing slip length) is no longer making significant difference on the oscillatory motion for both liquids.

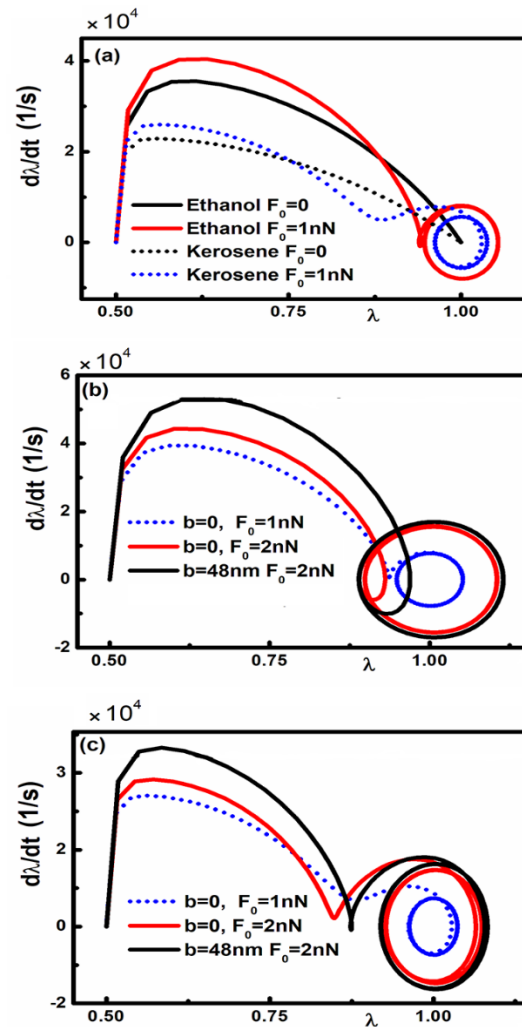


**Figure 8.** Phase portraits for the driven microsystem with an external applied force  $F_0\cos(\omega_d t)$  with  $\omega_d = 0.5\omega_0$ .  $z^* = 0.5d$ ,  $d = 300$  nm, and  $K = 0.05$  N/m are used. (a) Three–layer Au micro systems (containing ethanol or kerosene) under the presence and absence of external driven periodic force without slip length ( $b = 0$ ). Three–layer Au micro systems containing (b) ethanol and (c) kerosene under different applied driven periodic forces and various slip lengths as indicated.

#### 4. Conclusions

In this study, we investigated the actuation dynamics of a micro device consisting of Au-coated components with different intervening liquids between the actuating components under the influence of Casimir and separation-dependent dissipative hydrodynamic drag forces. This is accomplished via phase space portraits, which demonstrate that by increasing the dielectric response of the intervening layer, one can prevent the microdevice to come into stiction due to decreasing in magnitude Casimir forces. Using the phase portraits of a microsystem that is placed in vacuum or air, it has been shown how the presence of a liquid and, as a consequence, the additional dissipation term due the position dependent hydrodynamic drag force can significantly influence the actuation dynamics of MEMS/NEMS. By assuming vacuum or air between the actuating components, there are closed or open orbits inside the phase portraits providing evidence that the restoring force is sufficiently strong or very weak in order to preserve stable operation of the micro devices. In addition, it is shown how the reduction of the quality factor  $Q$  or, equivalently, by enhancing the Stoke energy dissipation can change an unstable motion towards stiction to stable dissipative motion.

However, by considering liquid (ethanol or kerosene) as the intervening medium, and as a consequence the existence of the additional hydrodynamic force between the components of MEMS the actuation dynamics changes drastically. Indeed, for both at the absence and presence of the external driven force, it is illustrated that it is feasible to expand area of motion using intervening liquids with lower dynamic viscosity or increasing the slip length (b) of the surrounding fluid leading to weaker hydrodynamic forces. It is indicated that the phase portraits related to the autonomous micro device containing liquid do not reveal closed orbit or, equivalently, continuous oscillation. Even by considering sufficiently strong restoring force, the phase portraits show spiral trajectory which eventually terminates the motion at a rest position. Finally, we investigated the influence of an external driven periodic force, which is the realistic case for device applications. It is demonstrated that the system can reveal continuous stable oscillation with an amplitude higher for the liquid that led to lower Casimir and hydrodynamic drag forces. Notably the amplitude of the driven force leads to significant influence on the continuous stable oscillation that takes place at relatively larger separations, while any decrease in hydrodynamic force via increasing the slip length has limited influence. Therefore, this study addresses the influence of the optical properties of the intervening layer for the three-layer actuating micro system. And the results presented in this study are essential for studying the dynamical behavior of three-layer micro devices, and for the designing and manufacturing of MEMS in order to operate in a stable manner in different environments.

**Author Contributions:** Writing—original draft: F.T.; Writing—review & editing: F.T. and G.P.; Formal analysis: F.T. All authors have read and agreed to the published version of the manuscript.

**Funding:** This research received no external funding.

**Data Availability Statement:** The data that support the findings of this study are available from the corresponding author upon reasonable request.

**Acknowledgments:** G.P. acknowledges support from the Zernike Institute for Advanced Materials, University of Groningen. F.T. acknowledges support from the Faculty of Physics, Alzahra University.

**Conflicts of Interest:** The authors declare no conflict of interest.

## References

1. Rodriguez, A.W.; Capasso, F.; Johnson, S.G. The Casimir effect in microstructured geometries. *Nat. Photonics* **2011**, *5*, 211–221. [[CrossRef](#)]
2. Capasso, F.; Munday, J.N.; Iannuzzi, D.; Chan, H.B. Casimir forces and quantum electrodynamic torques: Physics and nanomechanics. *IEEE J. Sel. Top. Quant. Electron.* **2007**, *13*, 400–414. [[CrossRef](#)]
3. Bordag, M.; Klimchitskaya, G.L.; Mohideen, U.; Mostepanenko, V.M. *Advances in the Casimir Effect*; Oxford University Press: Oxford, UK, 2015. [[CrossRef](#)]
4. Decca, R.S.; López, D.; Fischbach, E.; Klimchitskaya, G.L.; Krause, D.E.; Mostepanenko, V.M. Precise comparison of theory and new experiment for the Casimir force leads to stronger constraints on thermal quantum effects and long-range interactions. *Ann. Phys.* **2005**, *318*, 37–80. [[CrossRef](#)]
5. Decca, R.S.; López, D.; Fischbach, E.; Klimchitskaya, G.L.; Krause, D.E.; Mostepanenko, V.M. Tests of new physics from precise measurements of the Casimir pressure between two gold-coated plates. *Phys. Rev. D* **2007**, *75*, 077101. [[CrossRef](#)]
6. Ashourvan, A.; Miri, M.F.R.; Golestanian, R. Noncontact rack and pinion powered by the lateral Casimir force. *Phys. Rev. Lett.* **2014**, *98*, 140801. [[CrossRef](#)] [[PubMed](#)]
7. Miri, M.F.; Golestanian, R. A frustrated nanomechanical device powered by the lateral Casimir force. *Appl. Phys. Lett.* **2011**, *92*, 113103. [[CrossRef](#)]
8. Ashourvan, A.; Miri, M.F.; Golestanian, R. Rectification of the lateral Casimir force in a vibrating noncontact rack and pinion. *Phys. Rev. E* **2007**, *75*, 040103. [[CrossRef](#)]
9. DelRio, F.W.; de Boer, M.P.; Knapp, J.A.; Reedy, E.D.; Clews, P.J.; Dunn, M.L. The role of van der Waals forces in adhesion of micromachined surfaces. *Nat. Mater.* **2005**, *4*, 629–634. [[CrossRef](#)]
10. Serry, F.M.; Walliserand, D.; Maclay, G.J. The role of the Casimir effect in the static deflection and stiction of membrane strips in microelectromechanical systems. *J. Appl. Phys.* **1998**, *84*, 2501–2506. [[CrossRef](#)]
11. Serry, F.M.; Walliser, D.; Maclay, G.J. The anharmonic Casimir oscillator (ACO)—The Casimir effect in a model microelectromechanical system. *J. Microelectromech. Syst.* **1995**, *4*, 193–205. [[CrossRef](#)]

12. Palasantzas, G.; DeHosson, J.T.M. Phase maps of microelectromechanical switches in the presence of electrostatic and Casimir forces. *Phys. Rev. B* **2005**, *72*, 121409. [[CrossRef](#)]
13. Milonni, P.W. *The Quantum Vacuum. An Introduction to Quantum Electrodynamics*; Academic Press, Inc.: San Diego, CA, USA, 1994. [[CrossRef](#)]
14. Sciamia, D.W. The physical significance of the vacuum state of a quantum field. In *The Philosophy of Vacuum*; Saunders, S., Brown, H.R., Eds.; Clarendon Press/Oxford University Press: Oxford, UK, 1991; pp. 137–158. [[CrossRef](#)]
15. Casimir, H.B.G. On the Attraction between Two Perfectly Conducting Plates. *Indag. Math.* **1948**, *10*, 261–263. Available online: <https://dwc.knaw.nl/DL/publications/PU00018547.pdf> (accessed on 24 October 2023).
16. Lifshitz, E.M. The Theory of Molecular Attractive Forces between Solids. *Sov. Phys. JETP* **1956**, *2*, 73–83. Available online: <http://jetp.ras.ru/cgi-bin/e/index/e/2/1/p73?a=list> (accessed on 24 October 2023).
17. Ball, P. Feel the force. *Nature* **2007**, *447*, 772–774. [[CrossRef](#)] [[PubMed](#)]
18. Chan, H.B.; Aksyuk, V.A.; Kleiman, R.N.; Bishop, D.J.; Capasso, F. Quantum mechanical actuation of microelectromechanical systems by the Casimir force. *Science* **2001**, *291*, 1941–1944. [[CrossRef](#)]
19. Pawlowski, P.; Zielenkiewicz, P. The quantum Casimir effect may be a universal Force organizing the bilayer structure of the cell membrane. *J. Membr. Biol.* **2013**, *246*, 383–389. [[CrossRef](#)] [[PubMed](#)]
20. Svetovoy, V.B.; Postnikov, A.; Uvarov, I.; Stepanov, F.; Palasantzas, G. Measuring the dispersion forces near the van der Waals–Casimir transition. *Phys. Rev. Appl.* **2020**, *13*, 064057. [[CrossRef](#)]
21. Velichko, E.N.; Klimchitskaya, G.L.; Mostepanenko, V.M. Dispersion forces between metal and dielectric plates separated by a magnetic fluid. *Techn. Phys.* **2019**, *64*, 1260–1266. [[CrossRef](#)]
22. Sedighi, M.; Svetovoy, V.B.; Broer, W.H.; Palasantzas, G. Casimir forces from conductive silicon carbide surfaces. *Phys. Rev. B* **2014**, *89*, 195440. [[CrossRef](#)]
23. Tajik, F.; Sedighi, M.; Khorrami, M.; Masoudi, A.A.; Palasantzas, G. Chaotic behavior in Casimir oscillators: A case study for phase-change materials. *Phys. Rev. E* **2017**, *96*, 042215. [[CrossRef](#)] [[PubMed](#)]
24. Tajik, F.; Sedighi, M.; Babamahdi, Z.; Masoudi, A.A.; Waalkense, H.; Palasantzas, G. Sensitivity of chaotic behavior to low optical frequencies of a double-beam torsional actuator. *Chaos* **2019**, *29*, 093126. [[CrossRef](#)]
25. Tajik, F.; Palasantzas, G. Sensitivity of actuation dynamics of Casimir oscillators on finite temperature with topological insulator materials: Response of repulsive vs attractive interactions. *Phys. Lett. A* **2023**, *481*, 129032. [[CrossRef](#)]
26. Klimchitskaya, G.L.; Mohideen, U.; Mostepanenko, V.M. Pulsating Casimir force. *J. Phys. A* **2007**, *40*, F841–F847. [[CrossRef](#)]
27. van Oss, C.J.; Chaudhury, M.K.; Good, R.J. Interfacial Lifshitz-van der Waals and polar interactions in macroscopic systems. *Chem. Rev.* **1988**, *88*, 927–941. [[CrossRef](#)]
28. Munday, J.N.; Capasso, F. Precision measurement of the Casimir–Lifshitz force in a fluid. *Phys. Rev. A* **2007**, *75*, 0601062(R). [[CrossRef](#)]
29. Klimchitskaya, G.L.; Mohideen, U.; Nepomnyashchaya, E.K.; Velichko, E.N. Effect of agglomeration of magnetic nanoparticles on the Casimir pressure through a ferrofluid. *Phys. Rev. B* **2019**, *99*, 045433. [[CrossRef](#)]
30. Goubault, C.; Jop, P.; Fermigier, M.; Baudry, J.; Bertrand, E.; Bibette, J. Flexible magnetic filaments as micromechanical sensors. *Phys. Rev. Lett.* **2003**, *91*, 260802. [[CrossRef](#)]
31. Pekas, N.; Porter, M.D.; Tondra, M.; Popple, A.; Jander, A. Giant magnetoresistance monitoring of magnetic picodroplets in an integrated microfluidic system. *Appl. Phys. Lett.* **2004**, *85*, 4783–4785. [[CrossRef](#)]
32. Inglis, D.W.; Riehn, R.; Austin, R.H.; Sturm, J.C. Continuous microfluidic immunomagnetic cell separation. *Appl. Phys. Lett.* **2004**, *85*, 5093–5095. [[CrossRef](#)]
33. Nishat, S.; Jafry, A.T.; Martinez, A.W.; Awan, F.R. Paper-based microfluidics: Simplified fabrication and assay methods. *Sens. Actuators B Chem.* **2021**, *336*, 129681. [[CrossRef](#)]
34. Philip, J.; Laskar, J.M. Optical properties and applications of ferrofluids. *J. Nanofluids* **2012**, *1*, 3–20. [[CrossRef](#)]
35. Mao, L.; Elborai, S.; He, X.; Zahn, M.; Koser, H. Direct observation of closed-loop ferrohydrodynamic pumping under traveling magnetic fields. *Phys. Rev. B* **2011**, *84*, 104431. [[CrossRef](#)]
36. Lin, W.; Miao, Y.; Zhang, H.; Liu, B.; Liu, Y.; Song, B. Fiber-optic in-line magnetic field sensor based on the magnetic fluid and multimode interference effects. *Appl. Phys. Lett.* **2013**, *103*, 151101. [[CrossRef](#)]
37. Saga, N.; Nakamura, T. Elucidation of propulsive force of microrobot using magnetic fluid. *J. Appl. Phys.* **2002**, *91*, 7003–7005. [[CrossRef](#)]
38. Fannin, P.C.; Marin, C.N.; Malaescu, I.; Stefu, N. Microwave dielectric properties of magnetite colloidal particles in magnetic fluids. *J. Phys. Condens. Matter* **2007**, *19*, 036104. [[CrossRef](#)]
39. Qi, H.; Zhang, X.; Jiang, M.; Wang, Q.; Li, D. A method to determine optical properties of kerosene using transmission spectrum. *Optik* **2016**, *127*, 8899–8906. [[CrossRef](#)]
40. Svetovoy, V.B.; Van Zwol, P.J.; Palasantzas, G.; De Hosson, J.T.M. Optical properties of gold films and the Casimir force. *Phys. Rev. B* **2008**, *77*, 035439. [[CrossRef](#)]
41. Garcia, R.; Perez, R. Dynamic atomic force microscopy methods. *Surf. Sci. Rep.* **2002**, *47*, 197–301. [[CrossRef](#)]
42. Vinogradova, V.O. Drainage of a thin liquid film confined between hydrophobic surfaces. *Langmuir* **1995**, *11*, 2213–2220. [[CrossRef](#)]
43. Vinogradova, O.I.; Yakubov, G.E. Dynamic effects on force measurements. 2. Lubrication and the atomic force microscope. *Langmuir* **2003**, *19*, 1227–1234. [[CrossRef](#)]

44. Vinogradova, O.I.; Yakubov, G.E. Surface roughness and hydrodynamic boundary conditions. *Phys. Rev. E* **2006**, *73*, 045302. [[CrossRef](#)] [[PubMed](#)]
45. Neto, C.; Evans, D.R.; Bonaccorso, E.; Butt, H.J.; Craig, V.S.J. Boundary slip in Newtonian liquids: A review of experimental studies. *Rep. Prog. Phys.* **2005**, *68*, 2859–2897. [[CrossRef](#)]
46. Bonaccorso, E.; Butt, H.J.; Craig, V.S.J. Surface roughness and hydrodynamic boundary slip of a Newtonian fluid in a completely wetting system. *Phys. Rev. Lett.* **2003**, *90*, 144501. [[CrossRef](#)] [[PubMed](#)]
47. Zhu, L.; Attard, P.; Neto, C. Reliable measurements of interfacial slip by colloid probe atomic force microscopy. II. Hydrodynamic force measurements. *Langmuir* **2011**, *27*, 6712–6719. [[CrossRef](#)] [[PubMed](#)]
48. Granick, S.; Zhu, Y.; Lee, H. Slippery questions about complex fluids flowing past solids. *Nat. Mater.* **2003**, *2*, 221–227. [[CrossRef](#)]
49. Siria, A.; Drezet, A.; Marchi, F.; Comin, F.; Huan, S.; Chevrier, J. Viscous cavity damping of a microlever in a simple fluid. *J. Phys. Rev. Lett.* **2009**, *102*, 254503. [[CrossRef](#)]
50. Maali, A.; Bhushan, B. Slip-length measurement of confined air flow using dynamic atomic force microscopy. *Phys. Rev. E* **2008**, *78*, 027302. [[CrossRef](#)] [[PubMed](#)]
51. Pan, Y.; Bhushan, B.; Maali, A. Slip length measurement of confined air flow on three smooth surfaces. *Langmuir* **2013**, *29*, 4298–4302. [[CrossRef](#)] [[PubMed](#)]

**Disclaimer/Publisher’s Note:** The statements, opinions and data contained in all publications are solely those of the individual author(s) and contributor(s) and not of MDPI and/or the editor(s). MDPI and/or the editor(s) disclaim responsibility for any injury to people or property resulting from any ideas, methods, instructions or products referred to in the content.